Structures of microfilament destabilizing toxins bound to actin provide insight into toxin design and activity

John S. Allingham*, Angela Zampella†, Maria Valeria D'Auria†, and Ivan Rayment*‡

*Department of Biochemistry, University of Wisconsin, Madison, WI 53706-1544; and †Università degli Studi di Napoli ''Federico II'', 80131 Naples, Italy

Edited by Thomas D. Pollard, Yale University, New Haven, CT, and approved August 15, 2005 (received for review March 14, 2005)

Marine macrolides that disrupt the actin cytoskeleton are promising candidates for cancer treatment. Here, we present the actin-bound x-ray crystal structures of reidispongiolide A and C and sphinxolide B, three marine macrolides found among a recently discovered family of cytotoxic compounds. Their structures allow unequivocal assignment of the absolute configuration for each compound. A comparison of their actin-binding site to macrolides found in the trisoxazole family, as well as the divalent macrolide, swinholide A, reveals the existence of a common binding surface for a defined segment of their macrocyclic ring. This surface is located on a hydrophobic patch adjacent to the cleft separating domains 1 and 3 at the barbed-end of actin. The large area surrounding this surface accommodates a wide variety of conformations and designs observed in the macrocyclic component of barbed-end-targeting macrolides. Conversely, the binding pocket for the macrolide tail, located within the cleft itself, shows very limited variation. Functional characterization of these macrolides by using *in vitro* actin filament severing and polymerization assays demonstrate the necessity of the *N*-methyl-vinylformamide moiety at the terminus of the macrolide tail for toxin potency. These analyses also show the importance of stable interactions between the macrocyclic ring and the hydrophobic patch on actin for modifying filament structure and how this stability can be compromised by subtle changes in macrolactone ring composition. By identifying the essential components of these complex natural products that underlie their high actin affinity, we have established a framework for designing new therapeutic agents.

cytoskeleton | cytotoxins | macrolides | marine natural products

The importance of the actin cytoskeleton in pathogenic cellular processes such as angiogenesis, cell adhesion, cytokinesis, and metastasis has made it an attractive target for the development of anticancer drugs (1). Small molecule marine natural products that target actin filaments with high affinity and potently interfere with actin filament dynamics have been shown to display cytotoxicity against several forms of multidrug resistant tumors (2–7). For this reason, their candidacy as clinical chemotherapeutic treatments has gained significant attention (8).

Reidispongiolides and sphinxolides are closely related macrocyclic lactone constituents of New Caledonian marine sponges *Reidispongia coerulea* and *Neosiphonia superstes*, which bind actin with high affinity and exhibit potent cytotoxicity against numerous human cancer cells (3, 5, 6). Structurally, these compounds can be divided into two major parts (Fig. 1*A*). First, the acyclic side chain of reidispongiolides and sphinxolides, referred to as the ''tail,'' is comprised of a long, stereochemically complex aliphatic chain, which typically terminates with an *N*-methyl-vinylformamide moiety. The second major part of the compound, the macrocyclic ring, can exhibit considerable diversity in both size and side groups. Reidispongiolide A and B and sphinxolides B–D represent the most abundant forms isolated from these sponge species. Reidispongiolide C and sphinxolide F and G have been isolated as minor metabolites in which the *N*-methyl-vinylformamide moiety is replaced by a carboxyl group (7).

Reidispongiolides and sphinxolides are members of a wider class of macrolides that target the barbed-end of actin and exhibit cytotoxic properties. All of these compounds, which include the aplyronins, mycalolides (9, 10) ulapualides (11), halichondramides (12, 13), and kabiramides (12, 14) (Fig. 1*B*) share the characteristic of a macrocyclic ring and tail, where the primary region of variability within and between different families of macrolides is associated with the macrocyclic component. Little is known about the biosynthetic pathway of these compounds, the enzymes involved in their biosynthesis, or the chemical constraints on the final products. Likewise, it is unknown how actin can accommodate such a wide variety of molecular structures. The goal of this study is to broaden our understanding of the necessary components for activity to better characterize the mode of toxin interaction with actin and to provide a framework for more specialized structural designs for therapeutic purposes.

Recently, studies by Paterson *et al.* (15) proposed two possible stereochemical configurations for reidispongiolide A based on combined results from chemical synthesis and NMR analysis of three degradation fragments. We now report the x-ray crystal structures of reidispongiolide (Red) A and C and sphinxolide (Sph) B in complexes with actin together with measurements of their effects on actin filament dynamics. In addition to establishing the absolute stereochemical configuration assignment for these compounds, this study reveals the mechanism of microfilament destabilization, the structural features important for novel ligand design, and a simple explanation for why these toxins consist of a macrocyclic ring and a tail.

Methods

Actin Purification. Actin used in the crystallizations and low-speed centrifugation assays was obtained from rabbit muscle acetone powder as described in ref. 16.

Toxin Isolation and Purification. RedA and C, and SphB, G, and F were isolated from the sponge *Reidispongia coerulea* collected south of New Caledonia and extracted according to published protocols (6, 7). Kabiramide C (KabC) and halichondramide (Hal) were provided as a generous gift by Junichi Tanaka (University of Ryukyus, Okinawa, Japan) (13, 14, 16). Ulapualide A (UlaA) was provided as a generous gift by the late Paul Scheuer (University of Hawaii, Honolulu) (11).

Crystallization, Data Collection, and Refinement. RedA and SphB were individually mixed at a 1:1 molar ratio with G actin and then

This paper was submitted directly (Track II) to the PNAS office.

Abbreviations: Red, reidispongiolide; Sph, sphinxolide; KabC, kabiramide C.

Data deposition: The atomic coordinates and structure factors have been deposited in the Protein Data Bank, www.pdb.org [PDB ID codes 2ASM (reidispongiolide A), 2ASP (reidispongiolide C), and 2ASO (sphinxolide B)].

‡To whom correspondence should be addressed. E-mail: ivan_rayment@biochem.wisc.edu.

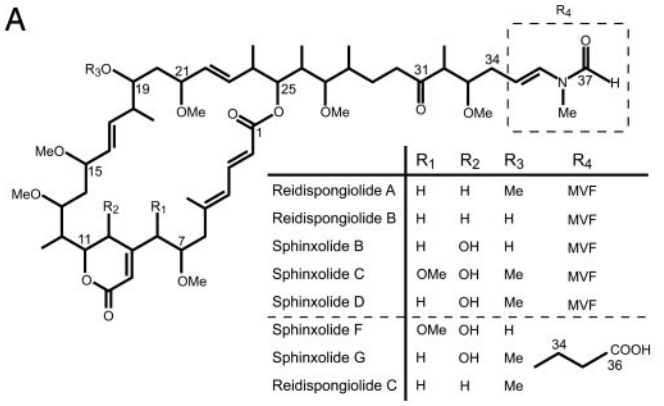

	R1	R2	R3	R4
Reidispongiolide A	H	H	Me	MVF
Reidispongiolide B	H	H	H	MVF
Sphinxolide B	H	OH	H	MVF
Sphinxolide C	OMe	OH	Me	MVF
Sphinxolide D	H	OH	Me	MVF
Sphinxolide F	OMe	OH	H	
Sphinxolide G	H	OH	Me	
Reidispongiolide C	H	H	Me	

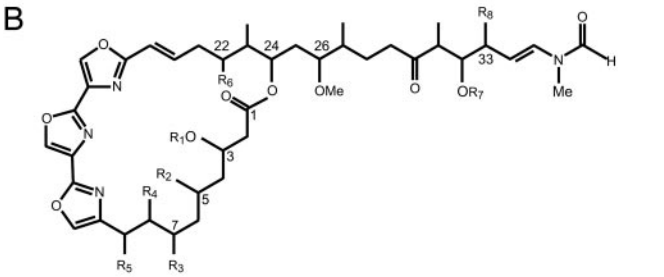

	R1	R2	R3	R4	R5	R6	R7	R8	Δ
Kabiramide C	$CONH_2$	Me	OH	Me	α-OMe	OMe	Me	Me	
Halichondramide	H	H	O	Me	β-OMe	H	Me	H	5,6
Jaspisamide A	H	OH	O	Me	β-OMe	H	Me	H	
Ulapualide A	H	H	O	H	α/β-OMe	OMe	Ac	Me	
Mycalolide A	H	H	O	Me	β-OMe	OMe	Ac	Me	5,6

Fig. 1. Molecular structure of selected marine macrolides from the reidispongiolide/sphinxolide and trisoxazole families. (*A*) Reidispongiolide/sphinxolide macrolides molecular structure. The boxed-in portion of the macrolide tail contains the highly conserved *N*-methyl-vinylformamide moiety (MVF) that is truncated and replaced by a carboxyl group in reidispongiolide C. (*B*) Trisoxazole macrolides molecular structure.

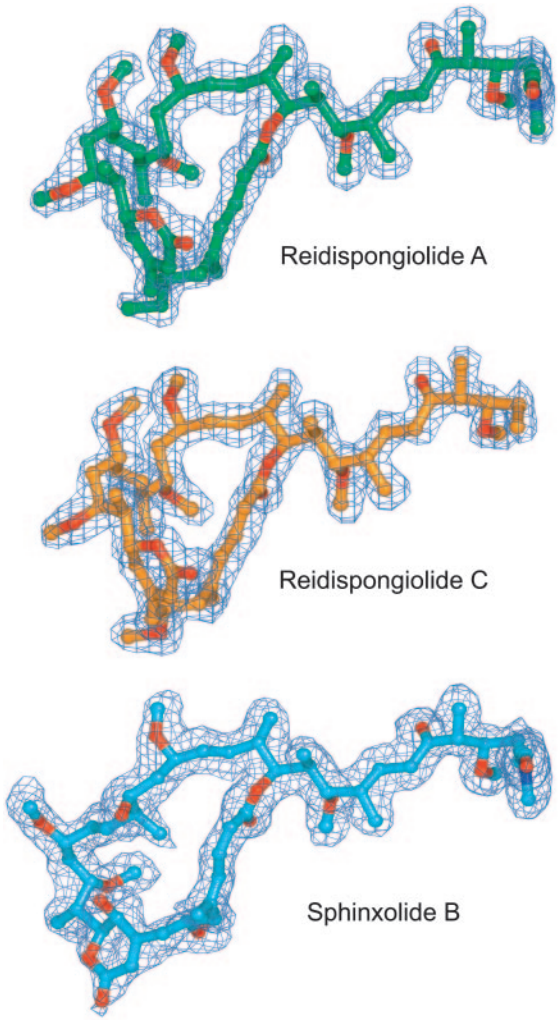

Fig. 2. RedA, RedC, and SphB structures and electron density. The F_o-F_c electron density omit maps for RedA, RedC, and SphB were contoured at 2.3σ, 2.5σ, and 2.0σ, respectively. The absolute stereochemistry of the chiral centers is defined as 7*R*, 11*R*, 12*R*, 13*S*, 15*S*, 18*S*, 19*S*, 21*R*, 24*S*, 25*S*, 26*S*, 27*S*, 28*S*, 32*R*, 33*R* for RedA and RedC, and 7*R*, 10*S*, 11*S*, 12*R*, 13*S*, 15*S*, 18*S*, 19*S*, 21*R*, 24*S*, 25*S*, 26*S*, 27*S*, 28*S*, 32*R*, 33*R* for SphB.

concentrated to 10–15 mg/ml. RedC was mixed with G actin at a 2:1 molar ratio. Crystals were grown and diffraction data were collected by using standard methods as described in *Supporting Text*, which is published as supporting information on the PNAS web site.

The structures of each complex were solved by molecular replacement starting from the actin–KabC structure (Protein Data Bank ID code 1QZ5; ref. 16). The structures were refined by using standard methods described in *Supporting Text*.

Actin Filament Capping and Severing Assays. Filament capping was performed with 9.0 μM of 15% pyrenyl-G actin (catalog no. AP05) from Cytoskeleton in G buffer in the presence or absence of 1 μM G actin–toxin complexes. Polymerization was initiated with 1/10th volume of Actin Polymerization buffer (500 mM KCl/20 mM $MgCl_2$/10 mM ATP; catalog no. BSA02-010). Pyrene fluorescence was monitored at 22°C by using a QuantaMaster C-60/2000 fluorimeter (Photon Technologies) with excitation and emission wavelengths of 365 and 407 nm, respectively. Gelsolin–actin seeds were assembled by mixing unlabeled G actin with full-length gelsolin at a 2:1 molar ratio in G buffer. Seeds were added to 9.0 μM pyrenyl-G actin for the capped filament polymerization assays at a final concentration of 0.18 μM. For analyses of F-actin severing, toxins were added at 24, 48, and 96 μM (final concentrations) to 100 μl of 48 μM rabbit skeletal muscle F actin in F buffer. The samples were incubated for 30 min at 4°C and then centrifuged at 20,000 $\times$ *g* for 30 min. The supernatant fraction was removed, and the pellets were resuspended in 100 μl of G buffer and analyzed by SDS/PAGE.

Results and Discussion

Stereochemical Assignment of RedA, RedC, and SphB. The structures of RedA, RedC, and SphB were solved as complexes with the Ca-ATP form of rabbit skeletal muscle actin by molecular replacement to a resolution of 1.6, 1.64, and 1.7 Å, respectively. A summary of the crystallographic statistics is presented in Table 1, which is published as supporting information on the PNAS web site. The electron density for each toxin allowed unequivocal assignment of their absolute stereochemical configurations (Fig. 2; see Fig. 7, which is published as supporting information on the PNAS web site). With the exception of an additional stereocenter at C10 for SphB, the absolute configurations at the remaining centers are identical. In the tail portion of RedC, the *N*-methyl-vinylformamide moiety is replaced by a carboxyl group at C36 (Fig. 1*A*); however, the electron density for the carboxylate moiety indicates that it adopts at least three different conformations that cannot be modeled with confidence.

Structures of Actin–Toxin Complexes. All three toxins bind at the barbed-end of actin, which adopts a similar conformation in all complexes (Fig. 8, which is published as supporting information on the PNAS web site). Furthermore, the conformation of actin observed here is closely related to that seen in the trisoxazole–actin complexes (16, 17), where, for example, the RMS differences between the Cα atoms of actin with RedA and SphB relative to KabC are 0.61 Å and 0.59 Å, respectively. Thus, the focus in this paper is the similarities and differences in the interaction of the toxins with actin, rather than the structure of actin itself.

In all of the complexes, the aliphatic tail of the macrolides make similar and extensive contacts with the bottom portion of the cleft separating actin subdomains 1 and 3. Conversely, the macrocyclic ring adopts two conformations. In the case of RedA and RedC, the macrolactone ring forms a close-knit interaction with a concave hydrophobic patch on the side of actin, whereas the ring of SphB displays a looser interaction with the same patch (Fig. 3*A*). The conformation observed for SphB appears to be stabilized by a crystal contact with a symmetry-related actin molecule (not shown).

The differences in the conformation of SphB relative to RedA and RedC are a consequence of the addition of an oxygen at C10 and absence of a methyl group on O19. Because of this addition, the approximate plane of the macrocyclic ring rotates by 100° where the changes originate as torsional rotation about the C3/C4 and C19/C20 of the macrocyclic ring. Interestingly, neither of the side groups associated with C10 or C19 interacts with actin in either toxin or alters the water structure, so the differences in conformation are not due to hydrophobic or polar interactions with actin. Rather, the altered conformation is due to changes in the conformational freedom of the toxin itself. Careful examination of the two toxins suggests that the introduction of an oxygen at C10, if it were to maintain the conformation observed for RedA, would introduce a close contact (≈2.8 Å) between O10 and C7. This unfavorable nonbonding interaction is absent in the structure of SphB (distance, 4.0 Å) because of changes in the torsional angles of 133° around the bond between C7 and C8. As a consequence of this restriction in the conformational freedom for SphB, its six-member lactone ring is no longer able to form the favorable hydrophobic and polar interaction observed in the complex with RedA. This finding illustrates the structural effect of ring substitutions on the binding of macrolides to actin. The biochemical consequence of these differences in ring substituents is described below.

Truncation of the *N*-methyl-vinylformamide moiety and its replacement by a carboxyl group at C36 in RedC results in the loss of several important hydrophobic interactions between C35 and Met-355, C36, and C37 and the aromatic ring of Tyr-169, and between the methyl group C47 and Tyr-133 that exist in RedA (Fig. 9, which is published as supporting information on the PNAS web site). Perhaps most important is the loss of the hydrogen bonding interactions formed by the bridging water molecules between O37 and the backbone amide hydrogens of Ile-136 and Ala-170 that stabilize the end of the tail in RedA and SphB (described in detail below). Combined with the loss of the double bond between C35 and C36 of the tail, these factors undoubtedly provide considerable rotational freedom to the end of the tail creating the observed disorder and weakening the interaction with actin.

Actin–Toxin Interfaces. RedA and C, and SphB occlude a large surface area on actin as was observed for the trisoxazole macrolides (16, 17) and more recently swinholide A (SwiA) (18). Comparison of the surface buried by RedA, RedC, SphB, and KabC shows that the primary source of binding stability for all these macrolides is due to hydrophobic interactions (Table 2, which is published as supporting information on the PNAS web site), where 60% of this surface area is provided by the aliphatic tail even though it contains fewer atoms than the macrocyclic ring.

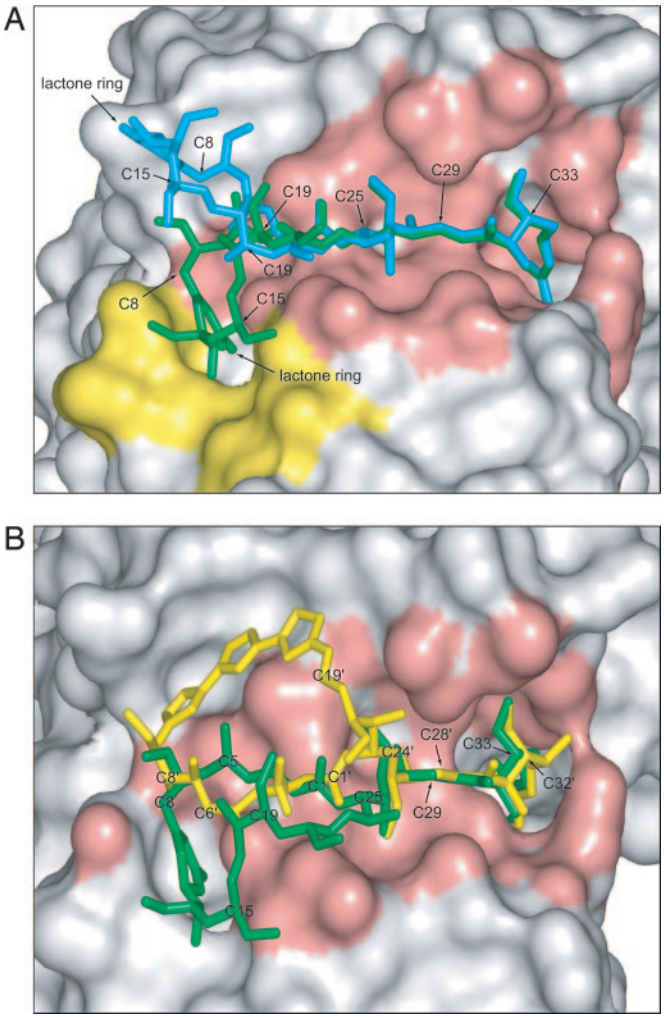

Fig. 3. Overlay of RedA, SphB, and KabC on actin. (*A*) RedA (green sticks) and SphB (cyan sticks) are shown superimposed in their actin-bound conformation on a surface drawing of actin. Common actin residue contacts are shown in salmon. Residues contacting RedA but not SphB are shown in yellow. Selected atoms and the lactone ring of each toxin have been labeled for reference. (*B*) RedA (green sticks) and KabC (yellow sticks) are shown superimposed in their actin-bound conformation. Residues that are common to the binding of both RedA and KabC are colored salmon. KabC atom numbers are given primes (′). The coordinates for KabC actin were obtained from Protein Data Bank entry 1QZ5. Toxins were superimposed on actin by using the program SUPERPOSE in CCP4.

The tail portions of the RedA and KabC bind to the cleft separating domains 1 and 3 with discernible conformational similarity (Fig. 3*B*) and involve nearly identical amino acid interactions (Fig. 4*A* and Figs. 9 and 10, which are published as supporting information on the PNAS web site). The highly conserved *N*-methyl-vinylformamide moiety is stabilized by two water molecules that are coordinated by the backbone amide hydrogens of Ile-136 and Ala-170. This interaction appears to be important for enhancing the stability of the actin–macrolide interaction as demonstrated by the biological properties of RedC, which lacks this moiety (described below).

The primary region of binding site variability between RedA, RedC, SphB, and the trisoxazole macrolides, such as KabC, is associated with their macrocyclic rings, which are chemically

BIOCHEMISTRY

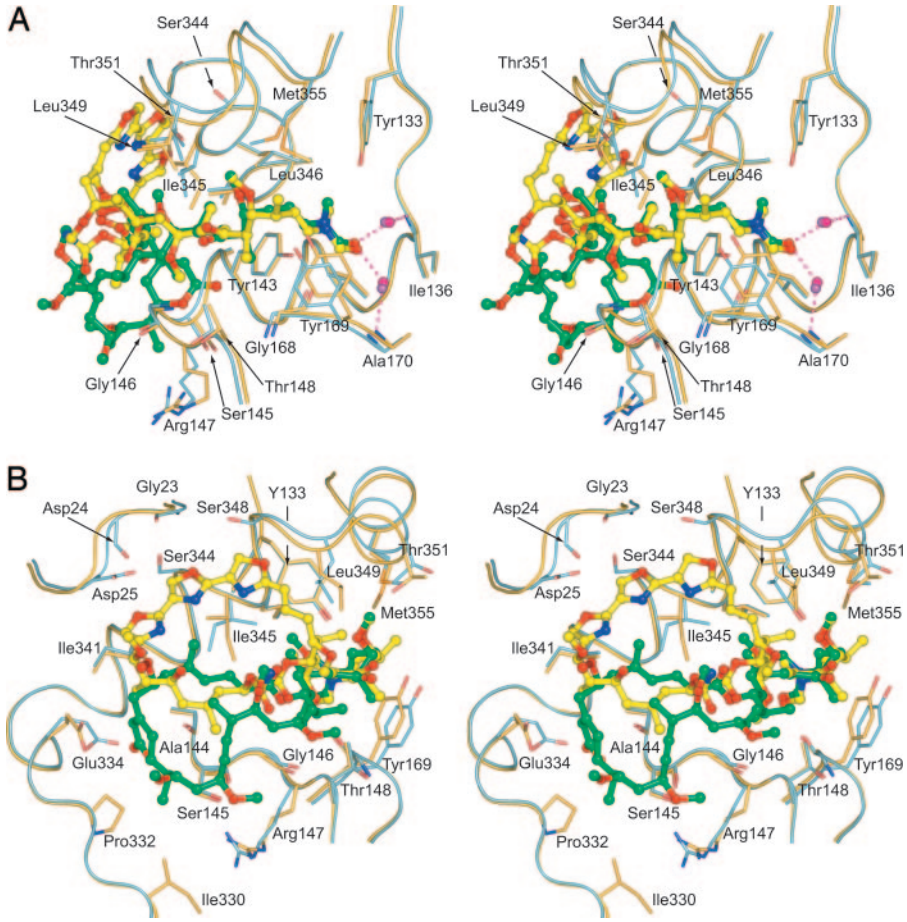

Fig. 4. RedA and KabC contacts on actin. (*A*) Stereoview of the tail portions of RedA (green ball and stick) and KabC (yellow ball and stick) bound to actin. RedA actin is shown in orange. KabC actin is shown in blue. Contact residues are shown as sticks. The *N*-methyl-vinylformamide moieties of RedA and KabC are depicted with bridging water molecules from each complex. Waters from the RedA–actin complex are pink; waters from the KabC–actin complex are violet. (*B*) Stereoview of the ring portions of RedA and KabC. Coloring is as described in *A*.

different and interact with unique regions of the hydrophobic patch (Figs. 4*B*, 9, and 10). Contacts unique to RedA include Ser-141, Ile-330, Pro-332, and Ser-338, whereas those unique to KabC include Gly-23, Asp-24, Asp-25, Ser-344, and Ser-348. Even so, they also share a common surface that appears to represent an important binding determinant on actin. The contacts common to both macrolides include Ala-144, Ser-145, Gly-146, Glu-334, Ile-341, and Ile-345. These contacts are made by a stretch of atoms (C1 to C8 in RedA and C1 to C9 in KabC) that lie in an extended conformation originating from the intersection of the ring and the tail. This interaction overlaps part of the "shear" region of actin that includes helix Ile-136 to Gly-146 (19, 20) and loop Arg-335 to Ser-338, below the ATP-binding site that has been implicated in conformational changes associated with nucleotide exchange. This finding suggests that the ring may inhibit nucleotide exchange (16). Interestingly, despite the different conformation observed for the macrolactone ring of SphB, the portion of the ring that remains in contact with actin includes the majority of this stretch of atoms (C1 to C6), which interact with actin in a similar manner to RedA. Furthermore, a structurally analogous portion of the macrocyclic ring of SwiA (18) is observed to interact with a similar binding patch in the complex with actin (Fig. 11, which is published as supporting information on the PNAS web site) and thus appears to be a universal feature of barbed-end actin-binding macrolides.

Toxin Ring and Tail Design Features Dictate Potency of Actin Filament Severing and Capping. Earlier studies have shown that the marine macrolides misakinolide A, mycalolide B, kabiramide D, and swinholide A exhibit potent microfilament severing and/or capping activity (21–23). Significant insight into the molecular basis for these activities has been provided by the recent solution of the actin-bound structures of several family members of these toxins (16–18, 24). It has been predicted that binding of the macrolide ring to the exposed hydrophobic patch between subdomains 1 and 3, followed by intercalation of the toxin tail into the cleft separating these domains, produces a complex that is incompatible with an interaction with the "lower" longitudinal actin protomer in the filament, leading to severing and capping of the broken filament (16, 25, 26). Here, using biochemical analyses on actin filament assembly and disassembly, we address the contributions made by the specific design features of these toxins during these events. Our results show that the *N*-methyl-vinylformamide moiety at the terminus of the tail is essential for formation of a stable interaction with actin. Furthermore, modulations of side groups found in the ring of SphB, which reduced the size of the actin-binding interface in the structure, correlated significantly with its effect on actin filament stability.

A low speed centrifugation assay of F actin filaments treated with the indicated ratios of toxin demonstrated that RedC, which lacks the *N*-methyl-vinylformamide moiety, was significantly less potent than RedA or halichondramide (Hal) at eliciting filament severing (Fig. 5). The effects of sphinxolide F and G, which also lack the *N*-methyl-vinylformamide group, were identical to RedC (data not shown). SphB was only marginally more potent than RedC at generating short filaments. In this case, although

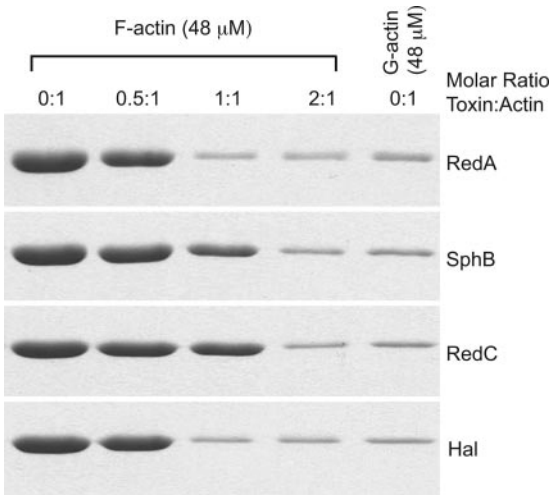

Fig. 5. Actin filament severing activity of marine macrolide toxins. One hundred microliters of F actin (48 μM) in F buffer was treated with the indicated molar ratio amounts of RedA, SphB, RedC, or Hal for 30 min and centrifuged at 20,000 $\times$ *g* for 30 min. The pellet of each sample after analysis by SDS/PAGE is shown. The pellets for G actin (48 μM) in G buffer without the addition of toxin are shown as a control for sedimentation of nonfilamentous actin within the tube.

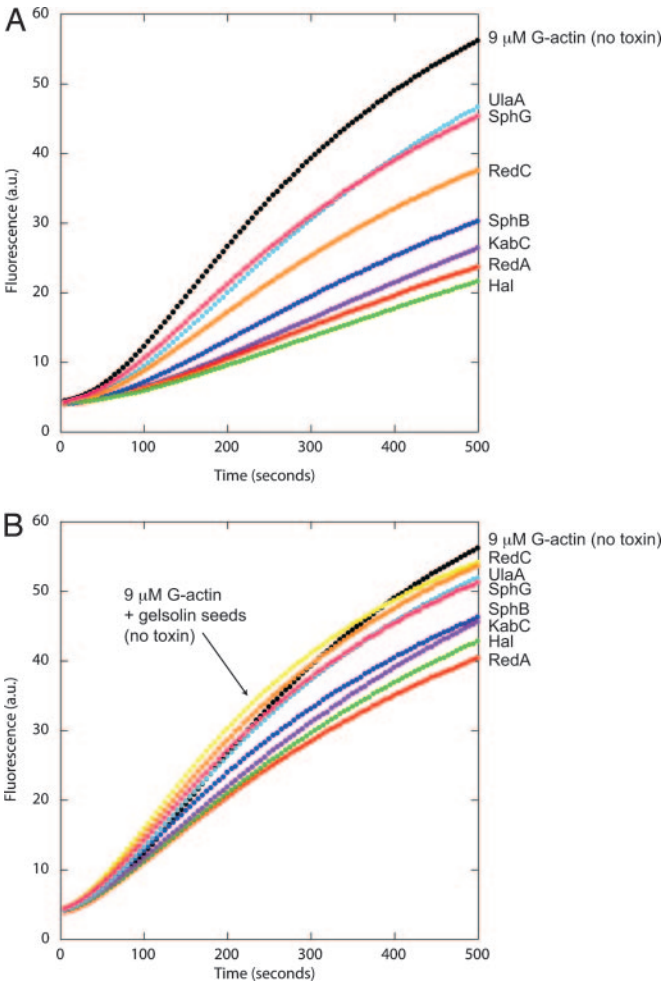

Fig. 6. Actin filament capping activity of marine macrolide toxins. Measurement actin polymerization by fluorescence intensity of pyrenyl-actin as a function of time. (*A*) G actin (9.0 μM) was mixed briefly with preformed 1 μM toxin–G actin complexes followed immediately thereafter by addition of KCl and $MgCl_2$. Polymerization reaction profiles are labeled according to the toxin–actin complexes added (black, 9.0 μM G actin without toxin–actin complexes; green, halichondramide; red, reidispongiolide A; purple, kabiramide C; blue, sphinxolide B; orange, reidispongiolide C; cyan, ulapualide A; pink, sphinxolide G). (*B*) G actin (9.0 μM) preincubated with 0.18 μM preassembled gelsolin-actin seeds. Control samples of 9.0 μM G actin only and G actin plus gelsolin seeds are shown in black and yellow, respectively. Profiles for reactions containing gelsolin seeds and 1 μM toxin–actin complexes are colored as in *A*.

having less of an impact than the absence of the *N*-methyl-vinylformamide moiety, the less extensive contacts observed between the macrolide ring and actin in the SphB–actin structure caused by the substitutions at C10 and O19 (Figs. 3*A* and 9) may have perturbed the efficiency at which SphB is able to make a stable interaction with the actin filament. It should also be noted that at the concentration of F actin used in this assay (48 μM), under polymerizing conditions, severed filaments can reanneal if not subsequently capped by the toxin. Therefore, we believe it is pertinent to state that this assay likely measures the efficiency of toxin-mediated severing as well as filament capping.

To explicitly ascertain the capping function of the toxins, we performed a kinetic assay involving time-dependent measurements of the increase of fluorescence intensity of pyrene-labeled actin upon filament polymerization in the presence and absence of preformed toxin–actin complexes. Toxins that inhibit polymerization of G actin have been shown to do so in two ways: by capping filament ends to prevent filament growth and/or by sequestering actin monomers to inhibit their ability to assemble onto growing filaments. Recent studies have demonstrated that the complex formed by KabC and actin behaves as an unregulated barbed-end-capping protein (24). Assuming the toxins form a 1:1 complex with G actin, inhibition of polymerization by sequestration should not have reduced the level of polymerization by more than that of the 9 μM G actin control. Here, we show that, in all cases, the addition of toxin–actin complexes produced a larger reduction in polymerization than could be predicted by sequestration alone, demonstrating their capping ability (Fig. 6*A*). Furthermore, similar to the toxins severing activity, the filament capping activity of the toxins is highly correlated to the presence of the *N*-methyl-vinylformamide group and a stable interaction between the ring and the hydrophobic surface on actin.

Analysis of the capping properties of the toxins performed in the presence of gelsolin-actin seeds, which act as nuclei promoting filament growth exclusively from the pointed-end (27), showed that the toxin–actin complexes compete with the gelsolin-actin seeds for the barbed-end of the filament during polymerization (Fig. 6*B*). Although the RedA, Hal, KabC, and SphB toxin–actin complexes moderately reduced the rate and level of polymerization relative to the control sample containing only gelsolin–actin seeds, the level of reduction was significantly less dramatic than for samples in which gelsolin was absent (Fig. 6*A*). We believe that the relatively minor effect of the addition of toxin is related to the toxin–actin complexes capping the barbed ends of actin dimers or trimers that form spontaneously after the addition of salt even in the presence of the gelsolin–actin seeds.

Functional Division of the Actin Binding Determinants in Marine Macrolides. All of the structural and biological evidence suggests that the aliphatic tail is a major contributor to the high affinity and functionality of the marine macrolides, where the stabilizing interactions include both hydrophobic and polar components. As shown here, coordination of the *N*-methyl-vinylformamide moiety is a key determinant of the efficiency with which the macrolide toxins bind actin filaments. In the absence of this moiety, as illustrated by the biochemical properties of RedC,

there is a significant reduction in the ability of this toxin to affect actin filament assembly and disassembly. Likewise, the minor effect on filament capping observed for ulapualide A (UlaA) is consistent with the importance of the interaction of actin with the *N*-methyl-vinylformamide group. In the latter case, UlaA retains this moiety, but it is disordered within the actin complex because of a substitution of the methyl at R7 (C32) by an acetate group (17), which prevents the interaction seen in other toxins. Pharmacological studies examining the activity of RedC, along with other truncated derivatives, shows a reduction in cytotoxicity toward various cancer cell types ranging from 10- to 100-fold relative to full-length sphinxolides (7) which confirms the biological importance of the interaction of actin with the *N*-methyl-vinylformamide group.

Compared to the aliphatic tail, the role and contribution of the macrocyclic ring to the actin affinity and biological function of these compounds was less clear given their variation in chemical structure. Indeed, the reason for a universal existence of a macrocyclic ring in these toxins was unknown, although an explanation is now apparent. The first nine atoms of all macrocyclic rings bind in an extended conformation to a shallow hydrophobic patch on the side of actin, whereas the bulk of the atoms in the rings adopt radically different orientations and make proportionately fewer interactions with actin. This finding suggests that this region on actin is a critical binding determinant, which is consistent with the reduced severing and capping ability of SphB that interacts less tightly with this region. We propose that the existence of a cyclic structure for these toxins was universally selected to reduce the conformational freedom of the unbound state of the toxin to enhance its interaction with a comparatively flat hydrophobic surface.

Conclusions. The mechanism of filament severing previously proposed by Klenchin *et al.* (16) in which binding of the toxins would disrupt the interaction between the stretch of hydrophobic residues in the DNase-binding loop of the "lower" axial actin protomer and the hydrophobic cleft separating domains 1 and 3 in the longitudinally related protomer, is consistent with the actin filament models proposed by Holmes and coworkers (16, 25, 26). Because our study shows that dissimilar toxins bind to the same area on actin, this finding means that we have defined a general site on actin that can be targeted by pharmacological agents. Importantly, none of the toxins observed so far have used all of the binding potential of this region. The overall size and shape of the targeted area indicates that a variety of solubility and specificity tags can be applied that should facilitate uptake and targeting. Together with the knowledge of the important binding determinants within marine toxins, these insights establish the foundation for designing novel structural analogues with enhanced biological activity.

We thank Dr. Vadim Klenchin for helpful discussions and Dr. Sofia Khaitlina for technical assistance with the filament dynamics assays. This work was supported by Canadian Institutes of Health Research Fellowship 64606 (to J.S.A.) and National Institutes of Health Grant AR35186 (to I.R.). Use of the SBC beamline Argonne National Laboratory Advanced Photon Source was supported by the U.S. Department of Energy, Office of Energy Research, under Contract No. W-31-109-ENG-38.

1. Giganti, A. & Friederich, E. (2003) *Prog. Cell Cycle Res.* **5,** 511–525.
2. Yeung, K. S. & Paterson, I. (2002) *Angew. Chem. Int. Ed. Engl.* **41,** 4632–4653.
3. Zhang, X., Minale, L., Zampella, A. & Smith, C. D. (1997) *Cancer Res.* **57,** 3751–3758.
4. Guella, G., Mancini, I., Chiasera, G. & Pietra, F. (1989) *Helv. Chim. Acta* **72,** 237–246.
5. D'Auria, M. V., Gomez-Paloma, L., Minale, L., Zampella, A., Verbist, J. F., Roussakis, C. & Debitus, C. (1993) *Tetrahedron* **49,** 8657–8664.
6. D'Auria, M. V., Gomez-Paloma, L., Minale, L., Zampella, A., Verbist, J. F., Roussakis, C., Debitus, C. & Patissou, J. (1994) *Tetrahedron* **50,** 4829–4834.
7. Carbonelli, S., Zampella, A., Randazzo, A., Debitus, C. & Gomez-Paloma, L. (1999) *Tetrahedron* **55,** 14665–14674.
8. Fenteany, G. & Zhu, S. (2003) *Curr. Top. Med. Chem.* **3,** 593–616.
9. Fusetani, N., Sugawara, T., Matsunaga, S. & Hirota, H. (1991) *J. Org. Chem.* **56,** 4971–4974.
10. Northcote, P. T., Blunt, J. W. & Munro, M. H. G. (1991) *Tetrahedron Lett.* **32,** 6411–6414.
11. Roesener, J. A. & Scheuer, P. J. (1986) *J. Am. Chem. Soc.* **108,** 846–847.
12. Matsunaga, S., Fusetani, N., Hashimoto, K., Koseki, K., Noma, M., Noguchi, H. & Sankawa, U. (1989) *J. Org. Chem.* **54,** 1360–1363.
13. Kernan, M. R. & Faulkner, J. D. (1987) *Tetrahedron Lett.* **28,** 2809–2812.
14. Matsunaga, S., Fusetani, N., Hashimoto, K., Koseki, K. & Noma, M. (1986) *J. Am. Chem. Soc.* **108,** 847–849.
15. Paterson, I., Britton, R., Ashton, K., Knust, H. & Stafford, J. (2004) *Proc. Natl. Acad. Sci. USA* **101,** 11986–11991.
16. Klenchin, V. A., Allingham, J. S., King, R., Tanaka, J., Marriott, G. & Rayment, I. (2003) *Nat. Struct. Biol.* **10,** 1058–1063.
17. Allingham, J. S., Tanaka, J., Marriott, G. & Rayment, I. (2004) *Org. Lett.* **6,** 597–599.
18. Klenchin, V. A., King, R., Tanaka, J., Marriott, G. & Rayment, I. (2005) *Chem. Biol.* **12,** 287–291.
19. Page, R., Lindberg, U. & Schutt, C. E. (1998) *J. Mol. Biol.* **280,** 463–474.
20. Dawson, J. F., Sablin, E. P., Spudich, J. A. & Fletterick, R. J. (2003) *J. Biol. Chem.* **278,** 1229–1238.
21. Bubb, M. R., Spector, I., Bershadsky, A. D. & Korn, E. D. (1995) *J. Biol. Chem.* **270,** 3463–3466.
22. Terry, D. R., Spector, I., Higa, T. & Bubb, M. R. (1997) *J. Biol. Chem.* **272,** 7841–7845.
23. Wada, S., Matsunaga, S., Saito, S., Fusetani, N. & Watabe, S. (1998) *J. Biochem. (Tokyo)* **123,** 946–952.
24. Tanaka, J., Yan, Y., Choi, J., Bai, J., Klenchin, V. A., Rayment, I. & Marriott, G. (2003) *Proc. Natl. Acad. Sci. USA* **100,** 13851–13856.
25. Holmes, K. C., Popp, D., Gebhard, W. & Kabsch, W. (1990) *Nature* **347,** 44–49.
26. Tirion, M. M., ben-Avraham, D., Lorenz, M. & Holmes, K. C. (1995) *Biophys. J.* **68,** 5–12.
27. Tellam, R. & Frieden, C. (1982) *Biochemistry* **21,** 3207–3214.